Accepted for publication in Proceedings of the Institution of Mechanical Engineers, Part F: Journal of Rail and Rapid Transit, Journal DOI: https://doi.org/10.1177/09544097221118456

Sources of variability in metro train-induced vibration

Xiangyu Qu[a,b] , David Thompson[b], Meng Ma[a,*], Minghang Li [c] and Evangelos Ntotsios[b]

[a] *School of Civil Engineering, Beijing Jiaotong University, Beijing 100044, China*

[b] *Institute of Sound and Vibration Research, University of Southampton, Southampton SO17 1BJ, UK*

[c] *Urban Rail Transit Center, China Academy of Railway Sciences Corporation Limited, Beijing, 100081, China*

Abstract

In previous in-situ measurements of metro trains it has been found that the velocity level on the track or tunnel wall may vary significantly between different train passages, even though the measuring section, the type of trains and the track and tunnel conditions are identical. An investigation is carried out into the sources of this variability, using a 3D train-track numerical model. This is built using the software SIMPACK and ABAQUS, and is connected through one-way coupling to a finite element model of the tunnel and soil. These models are used to study the influence of various train parameters, including the wheel and rail unevenness, train speed and degree of train loading. For comparison, in-situ measurements were made of the dynamic response of the rail and tunnel wall. The rail roughness at the site as well as the wheel unevenness of all 48 wheels for one train were measured. The results

from the model indicate that the wheel unevenness affects the rail velocity level in the frequency region between 25 and 250 Hz and tunnel wall vibration above 5 Hz. The rail velocity level can vary by up to 20 dB due to wheel unevenness, with the largest variations occurring in the frequency bands 50-63 Hz. Variations in passenger loading affect the train-induced vibration by up to 4.5 dB, mainly in the low frequency region. When the train speed varies within a range of ±20% relative to the nominal speed 60 km/h, the frequencies of the peaks are shifted and the level in some frequency bands can change by as much as 10 dB. However, the largest influence is that of the wheel unevenness. It is concluded that the variation in these parameters, especially the wheel and rail unevenness, should be considered to achieve reliable predictions of train-induced vibration.

Keywords: railway vibration; train conditions; rigid-flexible coupled model; wheel and rail unevenness; vibration excitation

1. Introduction

Railway transportation, especially urban metro systems, has developed rapidly in recent decades. However, disturbance due to ground vibration from railways is becoming increasingly problematic in urban areas, and forms a potential challenge for future metro construction. Train-induced vibration can cause disturbance to residents and can affect sensitive instruments in nearby buildings [1, 2].

To predict and reduce railway-induced vibration, evaluation and prediction methods have developed rapidly in recent years [3, 4]. These include empirical, analytical, and numerical methods. Empirical methods [5, 6] are often preferred due to their simple concept and high prediction efficiency. Analytical models [7-9] have a high computational efficiency and, although they may not have a high absolute accuracy due to their inherent approximations, they are useful for studying the relative effects of changes from one situation to another. Numerical methods in the time domain [10, 11] or in the frequency domain [12] are also widely used to predict train-induced vibration, and allow investigations of the effects of more complex variations in geometry or materials. Moreover, commercial software models based on multi-body analysis of trains have been widely used in engineering applications, such as the dynamic analysis of trains crossing bridges [13], analysis of track dynamics integrated with railway vehicle dynamics [14, 15], and inclusion of structural flexibility in vehicle dynamic systems [16, 17].

Despite the large variety of prediction methods available, most studies only predict a deterministic result, i.e. a particular vibration level or response spectrum due to one set of input parameters [18, 19]. In reality, the vibration is strongly affected by different types of uncertainty, for example in the train, track, and soil parameters, which can cause the vibration response to be distributed in a certain range instead of having a deterministic value [20]. In-situ measurement results, in particular, indicate that the vibration response varies significantly with different train passages even at a

single receiver point[21]. For the whole prediction path, the combined standard uncertainty was determined to be 3.9 dB(A)[22]. Furthermore, there are large differences between the vibration at different receiver locations due to variations in soil properties [23].

In the empirical methods, the tunnel wall vibration is often used to quantify the source level. Its value can be determined by averaged results from different train passages. However, if the differences in response caused by different trains are too large, the uncertainty and variability cannot be ignored. For a certain receiver position, the track type and train type are known and can be determined. Moreover, the rail unevenness can be assumed not to change in the short term (e.g. within the same day). Thus, the variability is mainly caused by differences between the conditions of each train; this is the subject of the present study. Features of the train that can vary include the wheel unevenness, the passenger loading and train speed.

Some authors have discussed the influence of train parameters on ground vibration from surface trains. Colaco et al. [24] performed a sensitivity analysis of the ground response by using a 2.5D finite element method (FEM) – boundary element method (BEM) approach for an Alfa Pendular type of train. They determined that the train unsprung mass had the most impact on vibration levels. Wheel/bogie spacing and semi-sprung mass, on the other hand, had no influence. Costa et al. [25] analysed the impact of different modelling assumptions on the calculated environmental vibration. They found that including only the wheelset mass in the model, and thereby

neglecting the suspension and the sprung mass of the train, had a significant influence on the environmental vibration responses between 5 and 15 Hz. This was due to the effect of the damping of the primary suspension. Milne et al. [26] studied the dependence of the load spectrum on train speed and axle spacings of intercity trains. For a train crossing a bridge, Mao et al. [27] discussed the dynamic response of the vehicle and the bridge under random variations in different train conditions; variations in train speed were based on the probability density evolution method. Mirza et al. [28] analysed different train parameters, e.g. vehicle mass, wheelset mass, suspension parameters and wheel spacing and their influence on ground vibration by using a fractional factorial design method for an intercity multiple unit train. However, these studies have focussed mainly on surface railways. The influence of train condition on rail and tunnel wall vibration response at a specific tunnel section needs further study.

Previous studies have shown that there can be quite large variations in the vibration level of the track and the tunnel, even for nominally similar trains. [23, 29, 30] The aim of the current study is to quantify the various potential sources of this uncertainty by using numerical simulations. The simulations are based on an example case of a B2 type metro train for which measurements are available. A 3D numerical model including train, track, tunnel and soil is used to investigate the variability in train-induced vibration, based on measurements of the unevenness of the train wheelsets and rail roughness. The results of varying different parameters describing

the train condition, in particular wheel unevenness, passenger loading and train speed, are presented and discussed.

2. Calculation model

To investigate the vibration under different train conditions, a 3D time-domain numerical model is built using the commercial software SIMPACK and ABAQUS. The model is divided into two parts. The train and track are represented by a coupled multibody dynamic (MBD) model of the vehicle and finite element (FE) model of the track, while the tunnel and soil are modelled by a finite element (FE) model, with infinite elements (IFE) to prevent reflections from the boundaries. In the first model, the measured wheel and rail unevenness data are used as inputs. The track is assumed to be located on a rigid foundation. The support forces in each rail fastening, calculated by using this model, are input to the second model as a series of time-varying loads. The two models are thus connected by a one-way coupling method in which the forces in each rail fastener are applied as excitation to the tunnel. This neglects any influence of the tunnel and ground on the track response, which is a reasonable assumption for a track with soft fasteners on a high impedance foundation. This technique is similar to the approach taken by Yang et al.[31] and Kouroussis et al.[32]. The velocity response of the rail in the first model and on the tunnel wall in the second model will be analysed.

2.1 Train-track MBD-FE coupled model

2.1.1 Train model

The train vehicle was considered as a multi-body dynamic system with 42 degrees of freedom. Some assumptions of the multibody train model are as follows:

(1) The elastic deformation of the vehicle components is neglected. This can be justified because flexible behaviour of the car body and bogie frames is isolated from the track by the vehicle suspension. Moreover, the wheel flexibility affects the response at frequencies above 300 Hz, which is not within the frequency range of concern for environmental vibration[33].

(2) The primary and secondary suspensions are regarded as massless spring-damper elements.

The nominal vehicle parameters used in the calculation are listed in Table 1. These are equivalent to a fully-loaded Chinese B2 type metro train. The most common metro train types in mainland China are the A-type and B-type trains, with the B-type trains being often used in new metro systems in recent years. The B2 type vehicle was selected for the current study because it is the most common train type used in Chinese metro systems. Moreover, the measurements of wheel unevenness and pass-by vibration described in Section 3 below were carried out on this type of vehicle.

Table 1 Nominal vehicle parameters. *x*, *y* and *z* represent the longitudinal, lateral and vertical directions.

Parameter	Direction	Motor car	Trailer
Car body length (m)		19.52	20.02
Distance between bogie centres (m)		12.6	12.6
Distance between wheelsets (m)		2.3	2.3
Wheel radius (m)		0.42	0.42
Vehicle body mass (kg)		35240	36060
Bogie mass (kg)		2973	1821
Wheelset mass (kg)		1494	1203
Moment of inertia of the vehicle body ($kg \cdot m^2$)	*x*	1.960×10^5	1.903×10^5
	y	1.297×10^6	1.316×10^6
	z	1.154×10^6	1.185×10^6
Moment of inertia of the vehicle bogie ($kg \cdot m^2$)	*x*	1206	1365
	y	1736	1190
	z	2809	2484
Moment of inertia of the vehicle wheelset ($kg \cdot m^2$)	*x*	706	652
	y	109	86
	z	716	652
Primary suspension stiffness (N/m)	*x*	1.517×10^6	1.517×10^6
	y	1.517×10^6	1.517×10^6
	z	1.203×10^6	1.203×10^6
Secondary suspension stiffness (N/m)	*x*	1.490×10^5	1.490×10^5
	y	1.490×10^5	1.490×10^5
	z	4.350×10^5	4.350×10^5
Primary suspension damping (Ns/m)	*z*	6000	6000
Secondary suspension damping (Ns/m)	*z*	6×10^4	6×10^4

2.1.2 Track model

A finite element model of the track was built using ABAQUS and input into SIMPACK based on the sub-model method to allow it to be coupled with the MBD train model. The track is represented by 68400 solid elements. It is assumed to be laid on a rigid foundation below the rail fasteners. A modal analysis was carried out, and the modes of the track structure were condensed to the main nodes by using the Guyan reduction method [34].

The length of the track model is 30 m with 50 fasteners on each rail. The spacing between fasteners is 0.6 m. The rail has a Young's modulus of 2.14×10^{11} Pa, density of 7850 kg/m^3, and Poisson's ratio of 0.3. The fasteners are modelled using spring and viscous damping elements, with the parameters chosen to represent $DTVI_2$ type fasteners, a type of directly fixed rail fastener system used in China. In the vertical direction, the stiffness is 8×10^7 N/m, with a damping factor of 7.5×10^4 N·s/m, whereas in the horizontal direction, the stiffness is 6×10^7 N/m, with a damping factor of 6×10^4 N·s/m.

2.1.3 Wheel/rail dynamic interaction

The train and track models are coupled in the time domain through SIMPACK's Flextrack module using nonlinear Hertzian contact theory to calculate the wheel/rail normal interaction forces. The time histories of the wheel and rail unevenness are

introduced in the Hertzian contact model as relative displacement inputs between the two bodies.

For modelling the wheel-rail contact in the tangential directions, the FASTSIM algorithm is used to represent the creep forces. This is an implementation of Kalker's steady-state simplified theory of rolling contact [35].

2.2 Tunnel-soil FE-IFE model

The track bed, tunnel, and soil are simulated based on the finite element method using ABAQUS, as shown in Figure 1. The size of the model is 40 m (length) × 40 m (width) × 50 m (height). The track bed and tunnel wall material is concrete, with density 2500 kg/m^3, Young's modulus 3.45×10^{10} Pa, Poisson's ratio 0.2, and damping ratio 0.05. The tunnel is considered as circular, with a diameter of 6 m and a lining thickness of 0.3 m. The buried depth of the tunnel is 10 m. The soil is treated as homogeneous and is included in the model only to provide support and suitable boundary conditions for the tunnel. The Poisson's ratio of the soil is 0.3, the compressional wave velocity is 255 m/s, the shear wave velocity is 137 m/s and the density is 2250 kg/m^3. The elements are 8-node linear brick elements (C3D8) with a maximum size of 0.1 m. At the boundaries of the FE domain, 8-node linear, one-way infinite brick elements (CIN3D8) are used to suppress wave reflections.

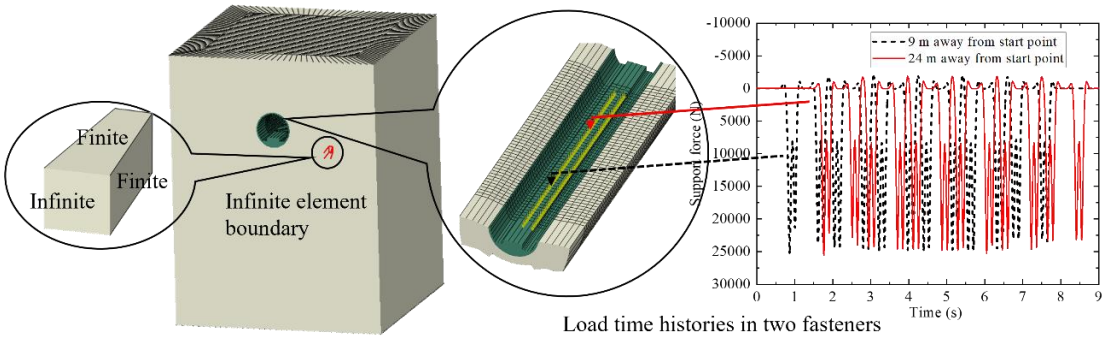

Figure 1. 3D FE-IFE model of tunnel and ground.

The forces in each rail fastener, as a function of time, can be obtained from the train-track model. Figure 1 displays examples of the time history of the force at two fasteners, one of which is 9 m from the start of the track and the other is 24 m from the start. These have similar waveforms but they are offset in time and also have different superimposed dynamic components due to the wheel and rail unevenness.

3. Comparison with measurements

3.1 Wheel and rail roughness measurements

The wheel unevenness was measured on all 48 wheels on one metro train in the depot. The train has six cars, including four motor cars and two trailers. The nominal radius of all the wheels is 0.42 m.

The TriTops instrument was used to obtain the wheel unevenness [36]. This has three probes with displacement sensors to measure the wheel profile at different lateral positions on the wheel tread simultaneously. They were located at 60, 70 and 80 mm from the back of the flange. The relative heights of the profile at the three sensors are preserved in the measurement. The profile from the middle probe position

is normalised to have an average height of 0, whereas probes 1 and 3 have an average height that is above or below 0. The mean of these three wheel unevenness traces is used to represent the input to the wheel/rail system.

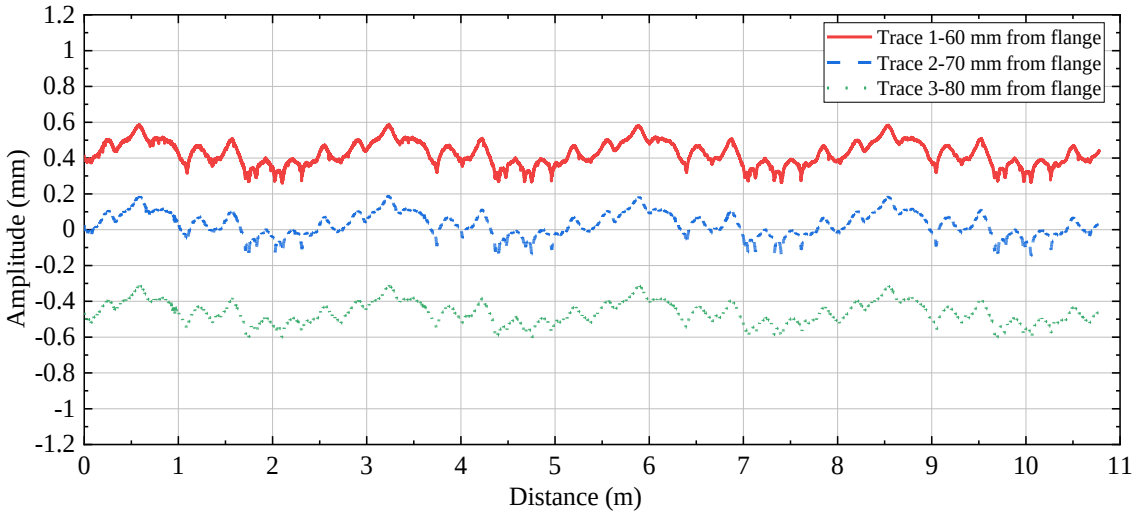

Figure 2. Example of wheel unevenness measured over four revolutions at three lateral positions. Trace 1 is at 60 mm from the flange back, trace 2 is at 70 mm and trace 3 is at 80 mm.

Figure 2 illustrates an example measurement obtained on wheel 8 of vehicle 2. Four revolutions of the wheel are shown in Figure 2 and the profile is plotted against running distance for three lateral positions. The amplitude indicates the relative height measured by the probe compared with the nominal rolling circle of the wheel.

The rail surface roughness was measured using a CAT (Corrugation Analysis Trolley). This instrument can continuously measure the rail surface roughness. The measured track distance is 60 m. The maximum wavelength obtained from the measurement data is approximately 1 m. For a nominal train speed of 60 km/h, the

corresponding frequency is 16.7 Hz. The minimum wavelength is 0.003 m, which is more than sufficient for the current purpose.

The acceleration vibration response of the rail and tunnel wall during train passages was measured at the same location as the rail roughness. Accelerometers were located vertically on the rail, and on the tunnel wall normal to the surface at 1 m above rail level. With the help of a digital data acquisition and analysis system, unattended intelligent acquisition was adopted, which automatically triggers, acquires, and stores data according to pre-set procedures. In this case, when the B2 type vehicles pass through this tunnel section, data on rail vibration and tunnel wall vibration are gathered. The nominal train speed at the test site was 60 km/h. The track type at the site is ballastless, with dimensions and material properties that correspond to the model parameters introduced in Section 2.2.

3.2 Comparison of measured and calculated results

The unevenness input into the MBD-FE model, as a function of distance, was derived from the measured left and right rail unevenness, and the measured wheel unevenness sample corresponding to the median of all the wheels.

Based on ISO 3095 [37], the measured unevenness can be expressed as the roughness level in one-third octave bands L_r^k (dB), which is expressed as:

$$L_{\mathrm{r}}^k = 10\log_{10}\frac{r_k^2}{r_{\mathrm{ref}}^2} \tag{1}$$

where r_{ref} is the reference value of the roughness level, 1 μm. r_k^2 is the mean square value of the roughness measured in the k-th one-third octave band. The one-third octave bands are expressed in terms of wavelength in mm. The mean value of all wheel roughness spectra, and the left and right rail roughness spectra are shown in Figure 3(a) in one-third octave bands. The rail and wheel roughness spectra have similar levels at most wavelengths.

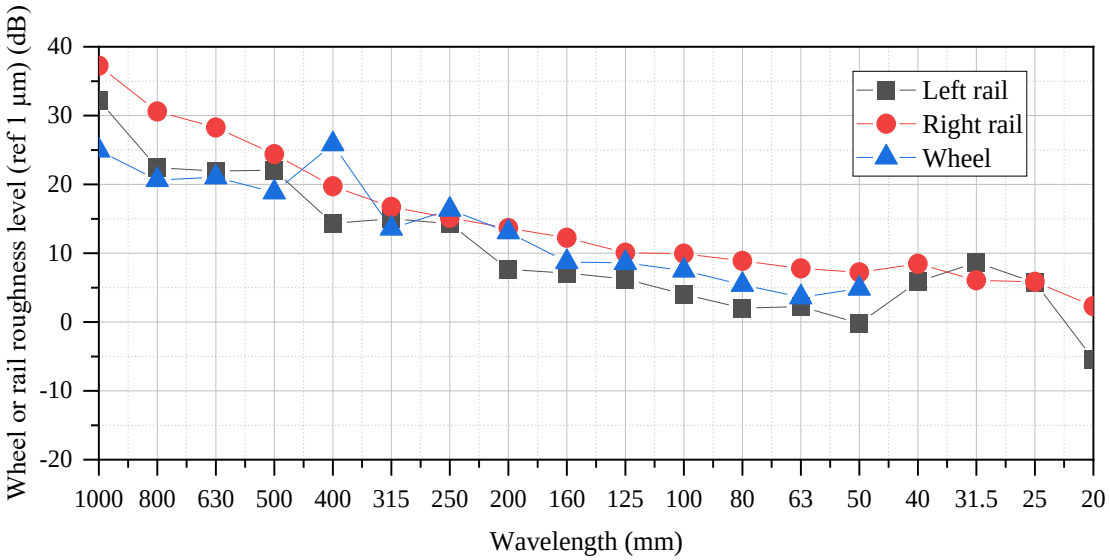

(a)

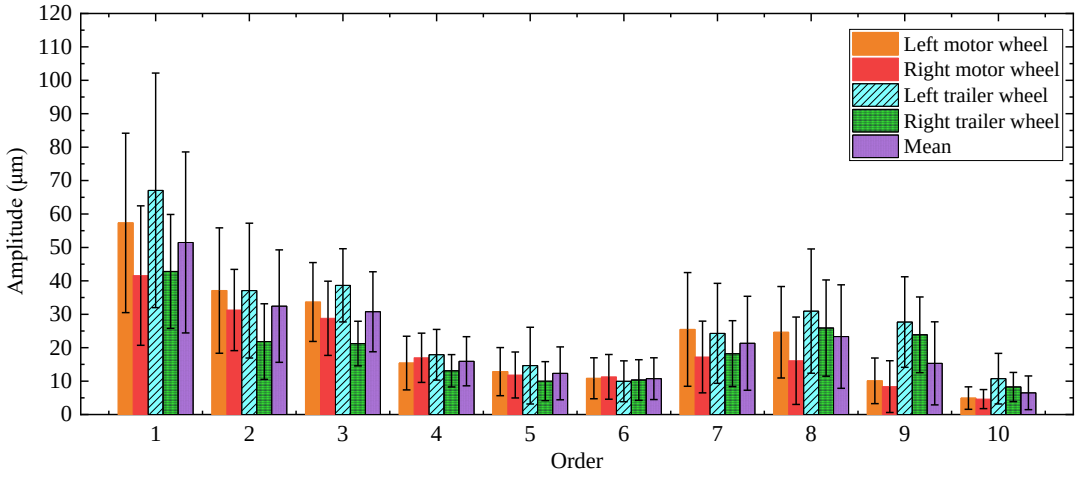

(b)

Figure 3. Measured unevenness data (a) Examples of wheel and rail unevenness spectra and (b) Wheel out-of-roundness orders.

The wheel out-of-roundness (OOR) orders are shown in Figure 3(b) as the average amplitudes of left and right motor wheels and left and right trailer wheels. There are differences in the unevenness of different wheels, but the main OOR orders are the first three and orders 7-9, as well as the error bar showing the range. The first order corresponds to a wavelength of 2.64 m, while the peak at order 7 corresponds to a wavelength of 0.38 m, also seen as a peak in the spectrum in Figure 3(a).

The calculation results were compared with the measured vibration responses on the rail and tunnel wall in terms of their frequency spectra. The total time simulated in the numerical model is 9 s, with a time step of 0.005 s. The results are converted into one-third octave spectra of velocity and compared with the measurements on the rail and on the tunnel wall. The calculated and measured velocity spectra are shown in Figure 4. These show reasonable agreement.

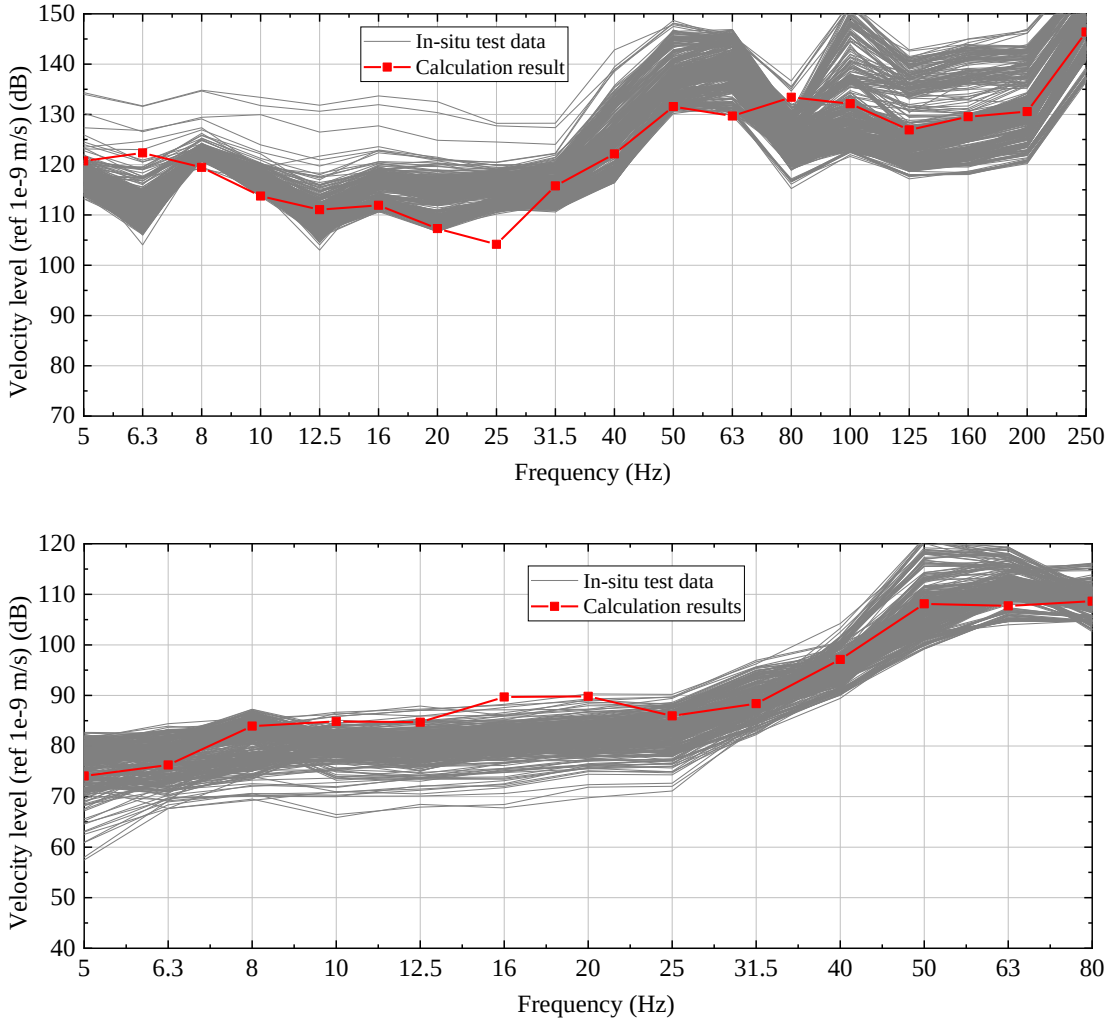

Figure 4. Comparison of results from the model with measurements (a) at rail (b) at tunnel wall.

4. Train condition parameters

To investigate the relationship between the train-induced vibration and the train condition, the influence of three main parameters is considered using the model: wheel unevenness, passenger loading and train speed.

4.1 Wheel unevenness

The measured wheel unevenness data together with the rail unevenness is input to the model. It is assumed that the wheels of one train are representative of the condition of all the trains passing the site.

The spectra of the measured wheel unevenness detected by all three probes for all 48 wheels are shown in Figure 5. Also shown are the mean spectrum of all these samples, and spectra of two samples that correspond approximately to the 5th percentile, representing a low level of wheel unevenness, and 95th percentile, representing a high level of wheel unevenness. As noted above, the wheels have a significant peak at the wavelength 400 mm.

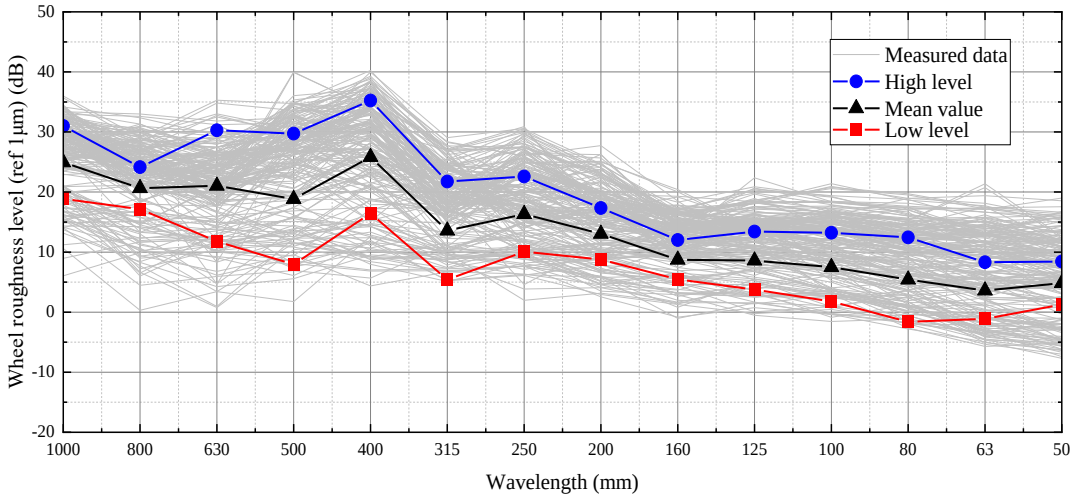

Figure 5. Wheel unevenness spectra of all wheels.

To study the influence of wheel unevenness, with and without rail roughness, the velocity responses on the rail and the tunnel wall were calculated for six different cases, as follows.

- Case 1: No wheel unevenness or rail surface unevenness.
- Case 2: Low-level measured wheel unevenness and no rail surface unevenness.
- Case 3: High-level measured wheel unevenness and no rail surface unevenness.
- Case 4: No wheel unevenness and measured rail surface unevenness.
- Case 5: Low-level measured wheel unevenness and measured rail surface unevenness.
- Case 6: High-level measured wheel unevenness and measured rail surface unevenness.

The low and high levels in Cases 2 and 3 (and also Cases 5 and 6) are chosen to correspond to the highlighted samples in Figure 5. The same wheel unevenness was applied to all wheels in the model.

The velocity levels on the rail and tunnel wall for these six cases are shown in Figure 6 in the form of one-third octave spectra. As expected, the lowest levels of vibration are obtained in Case 1 with neither wheel nor rail unevenness. Compared with this case, the rail vibration increases above 20 Hz and the tunnel wall vibration above 5 Hz when either wheel or rail unevenness is included. The vibration is unchanged at low frequency because the wheel and rail unevenness only influences the dynamic component of vibration and not the low frequency quasi-static component. From Cases 2 and 3, it can be observed that without any rail roughness,

there are differences in the rail vibration of around 10 dB, and in some bands up to 20 dB, between the results with the low-level and high-level wheel unevenness. When the measured rail roughness is included (comparing Case 4 with Cases 5 and 6), it can be observed that even under measured rail unevenness, the worst wheel unevenness can still significantly influence the vibration responses between 40 and 200 Hz on the rail and above 5 Hz at the tunnel wall. The level of variation is broadly consistent with the in-situ measurement data shown in Ref 30, which contained a measured distribution of 10 dB in the rail and tunnel wall vibration. It can be concluded that the wheel unevenness is a significant factor which influences the rail and tunnel wall vibration response and should not be ignored, especially when the track roughness level is low.

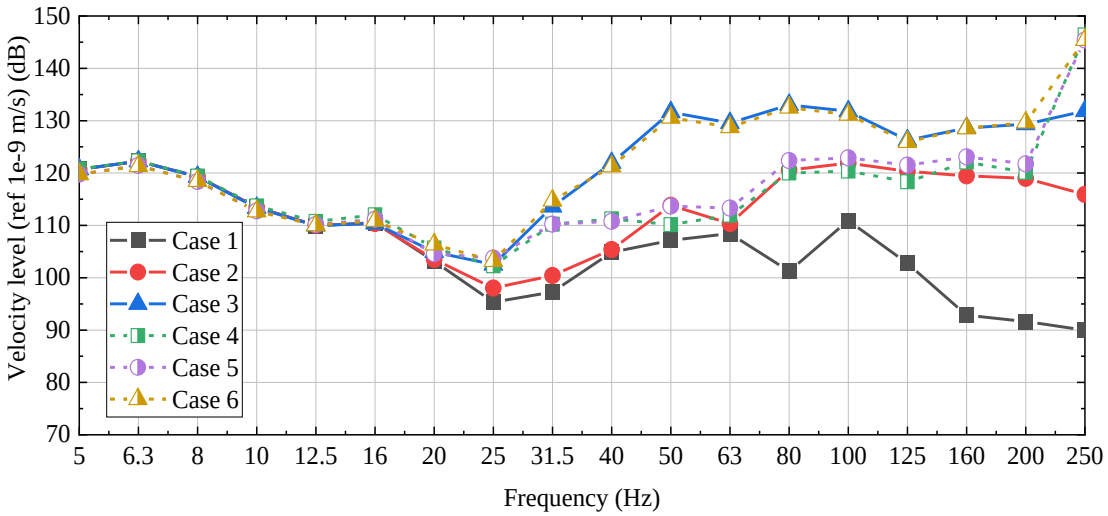

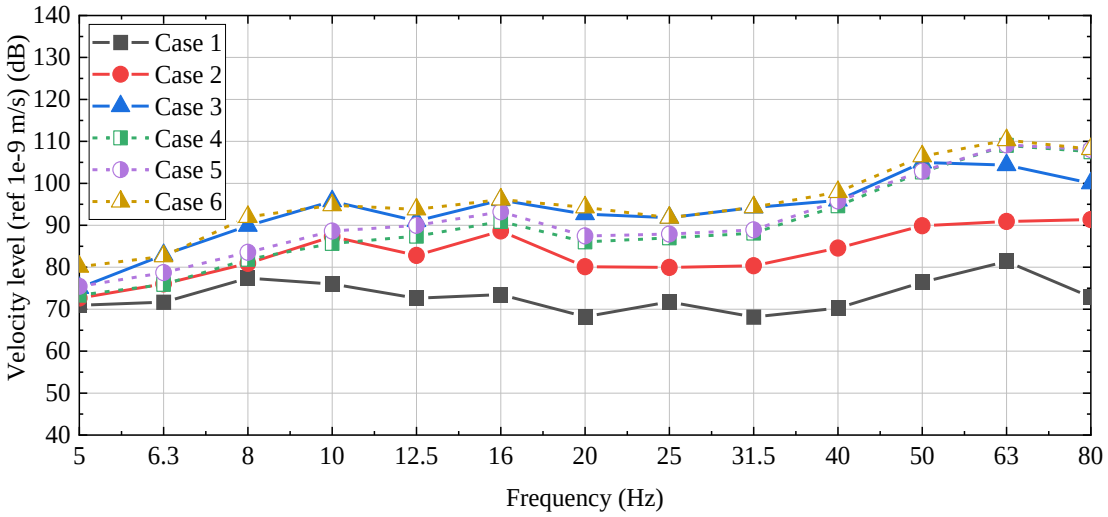

Figure 6. Velocity levels for different levels of wheel unevenness and rail unevenness (a) at rail (b) at tunnel wall.

4.2 Passenger loading

The number of passengers in a vehicle can affect the sprung mass and the total axle loads, which can then affect the rail and tunnel wall response. In the following calculation results, the mass and moment of inertia of the car body were adjusted to simulate different passenger loadings.

Three cases are considered: empty, with an axle load of 8 t; fully loaded, which means an axle load of 12 t with nominal passenger capacity (i.e., 6 persons/m^2); and crush loaded, which means an axle load of 14 t with excess passenger capacity (i.e., 9 persons/m^2). The fully loaded case corresponds to the nominal parameters introduced in Table 1. The other cases were generated by modifying the nominal body mass, moment of inertia, and secondary suspension stiffness. The details of these three cases are shown in Table 2.

Table 2 Vehicle parameters (empty/fully loaded/crush loaded)

Parameter	Direction	Case	Motor car	Trailer
Vehicle body mass (kg)		Empty	20000	22500
		Fully loaded	35240	36060
		Crush loaded	39500	39900
Moment of inertia of the vehicle body ($kg \cdot m^2$)	*x*	Empty	1.081×10^5	1.121×10^5
		Fully loaded	1.960×10^5	1.903×10^5
		Crush loaded	2.205×10^5	2.124×10^5
	y	Empty	7.725×10^5	9.013×10^5
		Fully loaded	1.297×10^6	1.316×10^6
		Crush loaded	1.443×10^6	1.433×10^6
	z	Empty	7.015×10^5	8.309×10^5
		Fully loaded	1.154×10^6	1.185×10^6
		Crush loaded	1.280×10^6	1.285×10^6
Secondary suspension stiffness (N/m)	*x*	Empty	1.180×10^5	1.180×10^5
		Fully loaded	1.490×10^5	1.490×10^5
		Crush loaded	1.690×10^5	1.690×10^5
	y	Empty	1.180×10^5	1.180×10^5
		Fully loaded	1.490×10^5	1.490×10^5
		Crush loaded	1.690×10^5	1.690×10^5
	z	Empty	2.450×10^5	2.450×10^5
		Fully loaded	4.350×10^5	4.350×10^5
		Crush loaded	4.650×10^5	4.650×10^5

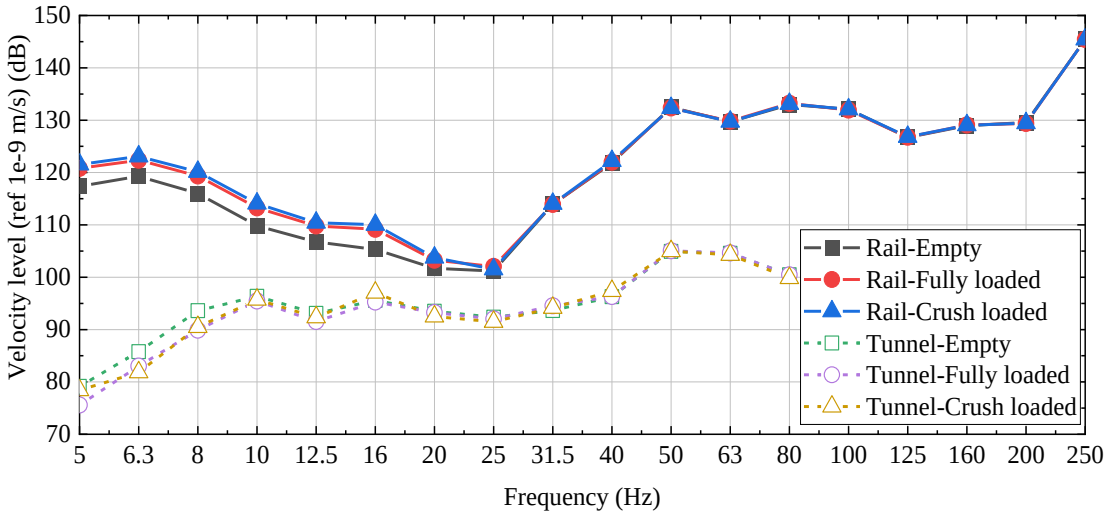

Figure 7. Velocity levels in 1/3 octave bands for different levels of vehicle loading at the rail and the tunnel wall.

Figure 7 compares the rail and tunnel wall velocity levels calculated using the high-level measured wheel unevenness (from Figure 5) for these different passenger loading cases. The number of passengers affects the vibration response below 25 Hz on the rail and below 10 Hz on the tunnel wall. The response in this frequency region is dominated by the quasi-static axle load and the vibration amplitude is proportional to the axle load[12]. Thus, it is expected that the response increases by 4.5 dB between the empty case and crush loaded case in this frequency region. However, at higher frequencies that are more important for ground-borne noise, the passenger loading has negligible effect.

4.3 Train speed

The sensitivity to the train speed is investigated by changing the speed by ±20% and ±10% relative to the nominal speed of 60 km/h. Therefore, the calculations are

performed for speeds of 72 km/h, 66 km/h, 54 km/h, and 48 km/h. The calculations are again carried out using wheel and rail unevenness from Case 6. All other vehicle parameters are assigned the nominal values from Table 1.

Figure 8 shows the velocity response of the rail and tunnel wall for these different train speeds. When the train speed increases from 48 km/h to 72 km/h, the frequencies corresponding to the response peaks increase (e.g., the peaks at 50 Hz and 80 Hz move to 63 Hz and 100 Hz). The amplitudes of the peaks do not change significantly for these moderate changes in the train speed in the frequency region 25-50 Hz. At lower frequencies, and in the region 50-80 Hz, the vibration response increases as the vehicle speed increases. In the 63 Hz band, and also around 8-10 Hz, the variation in the velocity level of the rail and tunnel wall may exceed 10 dB for this range of speeds.

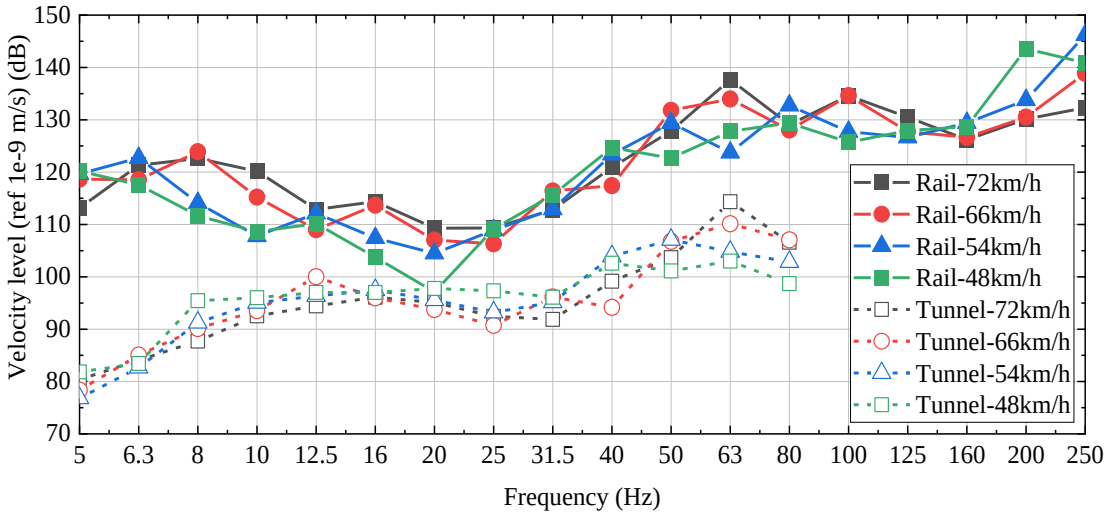

Figure 8. Velocity levels in 1/3 octave bands for different train speeds at rail and tunnel wall.

4.4 Discussion

Based on the calculation results from numerical model, the wheel unevenness, passenger loading and train speed are found to influence the train-induced vibration to different extents. Some previous experimental investigations on metro vibration variability [23, 30] have associated the dispersion of measured data between 25 and 200 Hz to differences in wheel unevenness. In this study, the variability in metro train-induced vibration is quantified by a numerical model. The results shown in this paper related to the mass of the vehicle are consistent with the investigation from Mirza et al.[28], who found that the mass of the vehicle mostly impacts the low frequency region, particularly 1-10 Hz. Mirza et al.[28] and Colaco et al. [24] also investigated other vehicle parameters such as wheelset mass, bogie mass and suspension stiffness and damping and wheel spacing. However, these have not been considered here as the investigation has focussed on variability in the measured vibration for a given type of vehicle. Moreover, wheel unevenness is found to have a larger effect on the vibration than unsprung mass and suspension parameters. Finally, in the current study on metro trains, the train speed was found to have only a small effect on the train-induced vibration. This is due to the low variation in speed in metro trains compared with the ranges considered for mainline trains in other investigations[27, 28].

5. Conclusions

The rail and tunnel wall vibration induced by different train conditions has been calculated using a 3D MBD-FE model. This time-domain model, which can consider the wheel and rail unevenness profiles as inputs, is suitable for investigating the influence of variable train conditions on train-induced vibration. The vibration responses under different conditions of wheel unevenness, passenger loading and train speed were discussed and the following conclusions are reached.

- For the nominal train speed, 60 km/h, the wheel unevenness mainly affects the rail vibration in the frequency region above 25 Hz and tunnel wall vibration above 5 Hz. The impact of the wheel unevenness on train-induced vibration is significant, especially in the frequency region 25-200 Hz. The rail velocity level can vary by up to 20 dB due to wheel unevenness, with the largest variations occurring in the frequency bands 50-63 Hz.
- The passenger loading in the train only controls the vibration of the rail in the frequency range below 25 Hz and the vibration of the tunnel in the frequency range up to 10 Hz, where the vibration is dominated by the quasi-static component.
- When the train speed varies within a range of ±20% relative to the nominal speed 60 km/h, the frequencies of the peaks are shifted. The velocity level at 63 Hz can increase by up to 10 dB when the train speed increased from 48 km/h to 72 km/h.

- At a certain receiver position, vehicles of the same type and nominal speed will still produce different vibration levels. This difference is mainly caused by the differences in wheel unevenness of each train.

Therefore, when predicting train-induced vibration, different train conditions need to be considered. This is not usually considered in conventional prediction methods which ignore variability in train conditions and directly obtain the average vibration from a single set of input parameters. Train conditions must be taken into account for more accurate predictions of train-induced vibration in advanced prediction models.

Acknowledgement

The authors acknowledge the help of Wanbo Li, Qingbin Li, and Yilei Xiong from Beijing Jiaotong University who participated in the measurements.

References

1. Sheng X. A review on modelling ground vibrations generated by underground trains. *International Journal of Rail Transportation* 2019; 7: 241-261. DOI: 10.1080/23248378.2019.1591312.
2. Thompson DJ, Kouroussis G and Ntotsios E. Modelling, simulation and evaluation of ground vibration caused by rail vehicles. *Vehicle System Dynamics* 2019; 57: 936-983. DOI: 10.1080/00423114.2019.1602274.
3. Kouroussis G, Vogiatzis KE and Connolly DP. A combined numerical/experimental prediction method for urban railway vibration. *Soil Dynamics and Earthquake Engineering* 2017; 97: 377-386. DOI: 10.1016/j.soildyn.2017.03.030.
4. Ma M, Xu L, Du L, et al. Prediction of building vibration induced by metro trains running in a curved tunnel. *Journal of Vibration and Control* 2021; 27: 515-528. DOI: 10.1177/1077546320930910.
5. Madshus C, Bessason B and Hårvik L. Prediction model for low frequency vibration from High-speed railways on soft ground. *Journal of Sound and Vibration* 1996; 193: 195-203. DOI: 10.1006/jsvi.1996.0259.

6. Hanson CE, Ross JC, Towers DA, et al. *High-speed ground transportation noise and vibration impact assessment*. 2012. United States. Federal Railroad Administration. Office of Railroad Policy and Development.
7. Sheng X, Jones C and Thompson D. A theoretical model for ground vibration from trains generated by vertical track irregularities. *Journal of sound and vibration* 2004; 272: 937-965.
8. Jones S and Hunt H. Predicting surface vibration from underground railways through inhomogeneous soil. *Journal of Sound and Vibration* 2012; 331: 2055-2069. DOI: 10.1016/j.jsv.2011.12.032.
9. Xu L and Ma M. Dynamic response of the multilayered half-space medium due to the spatially periodic harmonic moving load. *Soil Dynamics and Earthquake Engineering* 2022; 157: 107246. DOI: 10.1016/j.soildyn.2022.107246.
10. Kouroussis G, Verlinden O and Conti C. Influence of some vehicle and track parameters on the environmental vibrations induced by railway traffic. *Vehicle System Dynamics* 2012; 50: 619-639. DOI: 10.1080/00423114.2011.610897.
11. Connolly D, Giannopoulos A and Forde M. Numerical modelling of ground borne vibrations from high speed rail lines on embankments. *Soil Dynamics and Earthquake Engineering* 2013; 46: 13-19.
12. Jin Q, Thompson DJ, Lurcock DEJ, et al. A 2.5D finite element and boundary element model for the ground vibration from trains in tunnels and validation using measurement data. *Journal of Sound and Vibration* 2018; 422: 373-389. DOI: 10.1016/j.jsv.2018.02.019.
13. Li Y, Xu X, Zhou Y, et al. An interactive method for the analysis of the simulation of vehicle–bridge coupling vibration using ANSYS and SIMPACK. *Proceedings of the Institution of Mechanical Engineers, Part F: Journal of Rail and Rapid Transit* 2016; 232: 663-679. DOI: 10.1177/0954409716684277.
14. Bezin Y, Iwnicki SD, Cavalletti M, et al. An investigation of sleeper voids using a flexible track model integrated with railway multi-body dynamics. *Proceedings of the Institution of Mechanical Engineers, Part F: Journal of Rail and Rapid Transit* 2009; 223: 597-607. DOI: 10.1243/09544097jrrt276.
15. Dietz S, Hippmann G and Schupp G. Interaction of Vehicles and Flexible Tracks by Co-Simulation of Multibody Vehicle Systems and Finite Element Track Models. *Vehicle System Dynamics* 2016; 37: 372-384. DOI: 10.1080/00423114.2002.11666247.
16. Chaar N and Berg M. Vehicle-Track Dynamic Simulations of a Locomotive Considering Wheelset Structural Flexibility and Comparison with Measurements. *Proceedings of the Institution of Mechanical Engineers, Part F: Journal of Rail and Rapid Transit* 2006; 219: 225-238. DOI: 10.1243/095440905x8907.
17. Escalona JL, Sugiyama H and Shabana AA. Modelling of structural flexiblity in multibody railroad vehicle systems. *Vehicle System Dynamics* 2013; 51: 1027-1058. DOI: 10.1080/00423114.2013.786835.
18. Ma M, Liu W, Qian C, et al. Study of the train-induced vibration impact on a historic Bell Tower above two spatially overlapping metro lines. *Soil Dynamics and Earthquake Engineering* 2016; 81: 58-74. DOI: 10.1016/j.soildyn.2015.11.007.

19. Auersch L. Simple and fast prediction of train-induced track forces, ground and building vibrations. *Railway Engineering Science* 2020; 28: 232-250. DOI: 10.1007/s40534-020-00218-7.
20. Liang R, Liu W, Ma M, et al. An efficient model for predicting the train-induced ground-borne vibration and uncertainty quantification based on Bayesian neural network. *Journal of Sound and Vibration* 2021; 495. DOI: 10.1016/j.jsv.2020.115908.
21. Connolly DP, Alves Costa P, Kouroussis G, et al. Large scale international testing of railway ground vibrations across Europe. *Soil Dynamics and Earthquake Engineering* 2015; 71: 1-12. DOI: 10.1016/j.soildyn.2015.01.001.
22. Weber C and Karantonis P. Rail Ground-Borne Noise and Vibration Prediction Uncertainties. *Noise and Vibration Mitigation for Rail Transportation Systems*. 2018, pp.307-318.
23. Ma M, Liu W and Liu W. Research progress of prediction method and uncertainty of train-induced environmental vibration. *Journal of Traffic and Transportation Engineering* 2020; 20: 1-16.
24. Colaço A, Costa PA and Connolly DP. The influence of train properties on railway ground vibrations. *Structure and Infrastructure Engineering* 2016; 12: 517-534. DOI: 10.1080/15732479.2015.1025291.
25. Costa PA, Calçada R and Cardoso AS. Influence of train dynamic modelling strategy on the prediction of track–ground vibrations induced by railway traffic. *Proceedings of the Institution of Mechanical Engineers, Part F: Journal of Rail and Rapid Transit* 2012; 226: 434-450. DOI: 10.1177/0954409711433686.
26. Milne DRM, Le Pen LM, Thompson DJ, et al. Properties of train load frequencies and their applications. *Journal of Sound and Vibration* 2017; 397: 123-140. DOI: 10.1016/j.jsv.2017.03.006.
27. Mao J, Yu Z, Xiao Y, et al. Random dynamic analysis of a train-bridge coupled system involving random system parameters based on probability density evolution method. *Probabilistic Engineering Mechanics* 2016; 46: 48-61. DOI: 10.1016/j.probengmech.2016.08.003.
28. Mirza AA, Frid A, Nielsen JCO, et al. Ground Vibration Induced by Railway Traffic – The Influence of Vehicle Parameters. In: Maeda T (ed) *Proceedings of 10th International Workshop on Railway Noise, Nagahama, Japan, 18-22 October 2010, Notes on Numerical Fluid Mechanics and Multidisciplinary Design*. 2012, pp.259-266.
29. Kuo KA, Lombaert G and Degrande G. Quantifying Uncertainties in Measurements of Railway Vibration. *Noise and Vibration Mitigation for Rail Transportation Systems*. 2018, pp.155-166.
30. Ma M, Li M, Qu X, et al. Effect of passing metro trains on uncertainty of vibration source intensity: monitoring tests. *Measurement* 2022; 193. DOI: 10.1016/j.measurement.2022.110992.
31. Yang J, Zhu S, Zhai W, et al. Prediction and mitigation of train-induced vibrations of large-scale building constructed on subway tunnel. *Sci Total Environ* 2019; 668: 485-499. 2019/03/11. DOI: 10.1016/j.scitotenv.2019.02.397.
32. Kouroussis G, Verlinden O and Conti C. A two-step time simulation of ground vibrations induced by the railway traffic. *Proceedings of the Institution of Mechanical Engineers, Part C: Journal of Mechanical Engineering Science* 2012; 226: 454-472. DOI: 10.1177/0954406211414483.
33. Peng B, Iwnicki S, Shackleton P, et al. The influence of wheelset flexibility on polygonal wear of locomotive wheels. *Wear* 2019; 432: 102917.
34. Guyan RJ. Reduction of stiffness and mass matrices. *AIAA journal* 1965; 3: 380-380.

35. Kalker J. A fast algorithm for the simplified theory of rolling contact. *Vehicle system dynamics* 1982; 11: 1-13.
36. TriTops software user guide. *RailMeasurement Ltd* 2013.
37. ISO3095. *Railway Applications: Acoustics-Measurement of Noise Emitted by Railbound Vehicles*. International Organization for Standardization, 2013.